

Driving enhanced quantum sensing in partially accessible many-body systems

Utkarsh Mishra¹ and Abolfazl Bayat^{1,*}

¹*Institute of Fundamental and Frontier Sciences,
University of Electronic Science and Technology of China, Chengdu 610054, China*

(Dated: November 29, 2021)

The Ground-state criticality of many-body systems is a resource for quantum-enhanced sensing, namely the Heisenberg precision limit, provided that one has access to the whole system. We show that for partial accessibility, the sensing capabilities of a block of spins in the ground state reduces to the sub-Heisenberg limit. To compensate for this, we drive the hamiltonian periodically and use a local steady-state for quantum sensing. Remarkably, the steady-state sensing shows a significant enhancement in precision compared to the ground state and even achieves super-Heisenberg scaling for low frequencies. The origin of this precision enhancement is related to the closing of the Floquet quasienergy gap. It is in close correspondence with the vanishing of the energy gap at criticality for ground state sensing with global accessibility. The proposal is general to all the integrable models and can be implemented on existing quantum devices.

Introduction.— The high sensitivity of quantum systems to variations of their environment makes them superior sensors to their classical counterparts [1–8]. This is reflected in the Cramér-Rao inequality, which determines the precision limit of estimating an unknown field h , quantified by the standard deviation δh , through $\delta h \geq 1/\sqrt{MF}$, where M is the number of samples and F is the Fisher information [9, 10]. While the classical Fisher information scales as $F_C \sim N$ (standard limit), with N being the number of resources (e.g., number of particles) in the sensor, the quantum mechanics allows to go beyond this and achieve $F_Q \sim N^2$ (Heisenberg limit). Several quantum features are known to provide enhanced sensing precision: (i) entanglement in the special form of GHZ [11–15] or N00N [16–18] states; (ii) wave function collapse resulted from sequential measurements separated by intervals of free evolution [19–25]; and (iii) quantum criticality in many-body systems [26–32]. Any of these approaches have their advantages and disadvantages. If a d -dimensional many-body system operates near its critical ground state, the quantum Fisher information (QFI) of the *whole* system scales as $F_Q \sim N^{2/d\nu}$, where the ν characterizes the critical exponent for the divergence of the correlation length [33]. In the absence of global accessibility, one can only control a subsystem, which in general is a mixed state. A key question is: how does QFI scales with the subsystem size in a critical system? Besides, can the Heisenberg scaling be retrieved if the scaling becomes sub-Heisenberg, due to the mixedness of the subsystem?

Non-equilibrium dynamics of periodically driven many-body systems has been exploited for investigating the emergence of steady-state [34], time-crystals [35], topological systems [36, 37], entanglement generation [38–42], Floquet spectroscopy [43, 44], dynamically controlled quantum thermometry [45], and dynamical phase transitions [46–48]. The useful features of periodically driven many-body systems are: (i) any local subsystem reaches a steady-state; and (ii) the Floquet mech-

anism is applicable which simplifies the study of the dynamics. In non-integrable systems, a periodic field drives any small subsystem to a featureless infinite temperature thermal steady-state with no memory of the Hamiltonian parameters [49]. On the other hand, for integrable models, a non-trivial steady-state can be obtained that carries information about the Hamiltonian parameters [34, 38–42, 50–52]. An important, yet unexplored, open question is whether the local steady-states of periodically driven integrable systems can be used for enhancing the sensing precision in many-body sensors with partial accessibility.

In this paper, we address the above open problems by considering an XY spin chain for detecting a transverse magnetic field. We first find that in the absence of global accessibility, the sensing precision, even at the critical point, diminishes to sub-Heisenberg scaling. Then, we show that by applying a proper periodic transverse field and exploiting the local steady-states we can even achieve super-Heisenberg sensitivity. Remarkably, this enhanced sensing is not limited to the critical points of the system and exists for all the points across the phase diagram with a vanishing Floquet quasienergy gap. The protocol can be realized in existing quantum devices using simple measurements.

Model.— We consider quantum XY spin chain for measuring an unknown static transverse magnetic field h_0 . To manipulate the system for the desired accuracy we apply a periodic transverse field, $h(t)$, to the system. Therefore, the total Hamiltonian can be written as

$$H(t) = -\frac{J}{2} \sum_{i=1}^N \left[\left(\frac{1+\gamma}{2} \right) \sigma_i^x \sigma_{i+1}^x + \left(\frac{1-\gamma}{2} \right) \sigma_i^y \sigma_{i+1}^y \right] - \frac{(h_0 + h(t))}{2} \sum_i \sigma_i^z, \quad (1)$$

where, $\sigma^\Theta (\Theta = x, y, z)$ are the Pauli matrices, J (which is set to be 1 throughout the paper) is the exchange coupling, $-1 \leq \gamma \leq 1$ is the anisotropic parameter, and the periodic-boundary conditions, i.e., $\sigma_{N+1}^\alpha \equiv \sigma_1^\alpha$, is im-

posed. At time $t=0$, a periodic field of the form of $h(t)=h_1 \sin(\omega t)$ is applied to the system, where $\omega = 2\pi/\tau$ with τ being the time-period. The Hamiltonian $H(0)$ shows quantum criticality at $h_0=h_c$ such that $h_c/J=1$ for all values of γ [3]. We consider that system is initially prepared in the ground state of $H(0)$. However, as discussed in the Supplementary Materials (SM) [54], the proposed mechanism is general and works for other initial states. By switching the probe field $h(t)$ the initial state starts to evolve. The exact solution for the evolved is provided in the SM.

Sensing with global accessibility.— If one has access to the whole system, namely $|\Psi_0(t)\rangle$, then the QFI is given by $F_Q(t)=4\chi_F(t)$, where $\chi_F(t)=\langle\partial_{h_0}\Psi(t)|\partial_{h_0}\Psi(t)\rangle-|\langle\Psi(t)|\partial_{h_0}\Psi(t)\rangle|^2$. Especially for $H(0)$ the global QFI has been extensively studied and it was shown that at the ground state criticality it scales as $F_Q^{gs}=F_Q(0)\sim N^2$ [26–31, 33, 59–65] while away from the criticality it scales as $F_Q^{gs}=F_Q(0)\sim N$. We show this in the SM by simulating the QFI of the global system. In the rest of the letter, we focus on partial accessibility.

Sensing with partial accessibility.— In the absence of global accessibility, one has to rely on accessing a local block of size L with $L \ll N$. The partially accessible state of the system is described by the reduced density matrix obtained by tracing out all particles out of the block L , namely $\rho_L(t)=\text{tr}_{N-L}\left(|\Psi_0(t)\rangle\langle\Psi_0(t)|\right)$. The QFI of the state is given by [10]

$$F_Q = \sum_{r,s=1}^{2^L} \frac{2\Re(\langle\lambda_r|\partial_{h_0}\rho_L|\lambda_s\rangle\langle\lambda_s|\partial_{h_0}\rho_L|\lambda_r\rangle)}{\lambda_r + \lambda_s}, \quad (2)$$

where, $\rho_L = \sum_{r=1}^{2^L} \lambda_r |\lambda_r\rangle\langle\lambda_r|$ with λ_r and $|\lambda_r\rangle$ being the eigenvalues and eigenvectors of ρ_L , respectively. $\Re[\cdot]$ denotes the real parts of the quantity inside the parenthesis and the sum excludes terms for which $\lambda_r + \lambda_s = 0$. Note that the QFI is independent of the choice of the measurement operators and, in general, depends on the unknown parameter h_0 . Calculation of the QFI for the state ρ_L is given in the SM

Steady-state of a block.— After a long-time t , the reduced density matrix $\rho_L(t)$ equilibrates to a steady-state. Our goal in this paper is to measure the QFI for such a steady-state. By using $H(t+\tau)=H(t)$ and Floquet formalism, one can obtain the time-evolved state after n -cycles from an initial state $|\Psi_0\rangle$ as $|\Psi(n\tau)\rangle = \sum_i e^{-i\mu_i n\tau} |\mu_i\rangle\langle\mu_i|\Psi_0\rangle$. Here $\{\mu_i, |\mu_i\rangle\}$ are the eigenvalues (Floquet quasienergies) and eigenvectors of the one-period Floquet operator $U(\tau)=\mathcal{T}e^{-i\int_0^\tau H(t)dt}$, with \mathcal{T} being time-order operator. The expectation value of a local operator, \mathcal{O} , in the time-evolved state then can be expressed as $\langle\mathcal{O}\rangle = \sum_\ell \langle\mu_\ell|\mathcal{O}|\mu_\ell\rangle|\langle\mu_\ell|\Psi_0\rangle|^2 + \sum_{\ell\neq j} \langle\mu_\ell|\mathcal{O}|\mu_j\rangle\langle\mu_\ell|\Psi_0\rangle\langle\Psi_0|\mu_j\rangle e^{-2i(\mu_\ell-\mu_j)n\tau}$. The first and second terms describe the diagonal contribution and

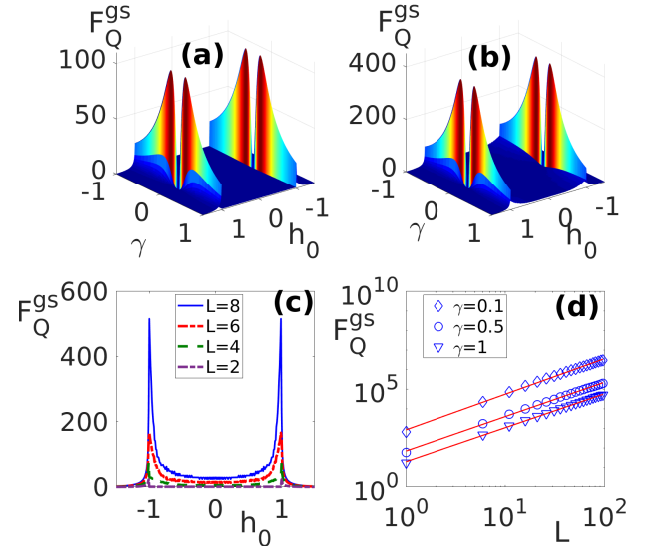


FIG. 1: The QFI of the ground state, F_Q^{gs} , as a function of γ and h_0 for (a) $L=2$ and (b) $L=4$. (c) The F_Q^{gs} as a function of h_0 when $\gamma=1$ for various choices of L . (d) The log-log scaling of F_Q^{gs} as a function of L for different γ 's. The fitting is shown by regular line whereas the markers represent the original data. In all panels $N=6000$.

the fluctuation around the diagonal term, respectively. The second term vanishes for a long time (Riemann-Lebesgue lemma). Using the above formalism, we calculate the expectation value of the fermionic correlation functions in the limit $t \rightarrow \infty$. (see SM for obtaining the local steady-state of the model). These correlation functions give the steady-state QFI, namely $F_Q^{ss} = \lim_{t \rightarrow \infty} F_Q(t)$ for the state ρ_L .

Ground state sensing.— In the absence of global accessibility, one has to rely on the sensing capability of ρ_L , which in general is a mixed state. This mixedness can diminish the sensing capability. To quantify this, we consider the ground state of $H(0)$ for $N=6000$ and plot the QFI, namely F_Q^{gs} , for $L=2$ and $L=4$ in Figs. 1(a) and (b), respectively. It can be seen from the plots that F_Q^{gs} shows peaks at points $h_0/J = \pm 1$ that marks the quantum criticality of the system. It is an interesting observation that not only the QFI of a full chain but also that of the reduced state distinguishes the criticality [26, 31, 66–68]. In Figs. 1(a) and (b), the F_Q^{gs} becomes vanishingly small at $\gamma=0$. Since for $\gamma=0$, the field part of $H(0)$ commutes with the interaction part, the variation of the field h_0 does not induce any change in the ground state of $H(0)$ which reflects itself in $F_Q^{gs}=0$. To have a better understanding of the role of L , we plot F_Q^{gs} versus h_0 at $\gamma=1$ in Fig. 1(c) for various L 's. The QFI increases with L and this effect becomes even more pronounced at the critical point $h_0/J = \pm 1$. To have a quantitative analysis for the scaling of the QFI at the critical point, in Fig. 1(d) we plot F_Q^{gs} as a function of L for $\gamma=0.1, 0.5, 1$ by fixing $h_0/J=1$. The scaling fol-

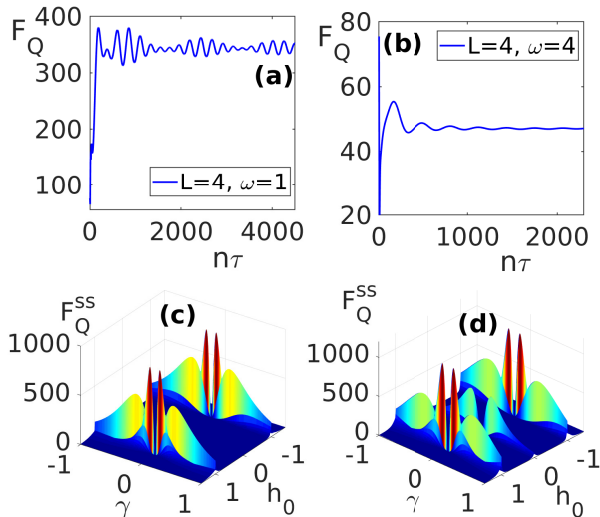


FIG. 2: F_Q as a function of time $t=n\tau$ for (a) $\omega=1$ (b) $\omega=4$, for $L=4$, $h_0/J=1$, and $\gamma=1$. Steady-state F_Q^{ss} as a function of h_0 and γ for (c) $\omega=4$ and (d) $\omega=2$. In all panels, the system size is $N=6000$ and $h_1=1.5$.

lows a power-law form, i.e., $F_Q^{gs}(h=h_c) \sim aL^\eta$. Numerical fitting results in $(a, \eta)=(6.718, 1.8)$ for $\gamma=0.1$, $(a, \eta)=(4.2235, 1.76)$ for $\gamma=0.5$, and $(a, \eta)=(2.967, 1.74)$ for $\gamma=1$, respectively. Thus, for the critical ground state and with partial accessibility, the QFI scales weaker than the Heisenberg bound (i.e., $\eta=2$), although it still outperforms the standard limit (i.e., $\eta=1$) showing quantum-enhanced sensing. Is it possible to improve this and retrieve Heisenberg scaling?

Steady-state sensing.— To enhance the sensing capability with $\rho_L(t)$, we propose to apply a periodic drive as given in Eq. (1). The resulting dynamics tend to thermalize the quantum state of the block. In non-integrable systems, while the global quantum state can still be used for quantum sensing [69, 70], the subsystems equilibrate to an infinite temperature state, and carry no information about the Hamiltonian [49]. In integrable models, as in Eq. (1), the steady-state does *not* thermalize to the infinite temperature due to local conserved quantities, and thus, carries a wealth of information about the parameters of the system [34]. To find the sensing capability of the steady-state of a block of $L=4$, in Figs. 2(a)-(b) we plot $F_Q(n\tau)$ as a function of time $t=n\tau$ for $\omega=1, 4$, respectively. The QFI reaches an equilibrium after a short transition time. Equilibration of the probe state is of multifold importance: (i) the imprinted information of h_0 in the density matrix may enhance the sensitivity and (ii) the emergent steady-state remains almost fixed in time which simplifies the measurement.

To see the sensing capability of the steady-state for a choice of $h_1=1.5$ and $L=4$, we compute the steady-state QFI, denoted as F_Q^{ss} . In Fig. 2(c), we plot F_Q^{ss} as a function of γ and h_0 for $\omega=4$. The F_Q^{ss} shows similar

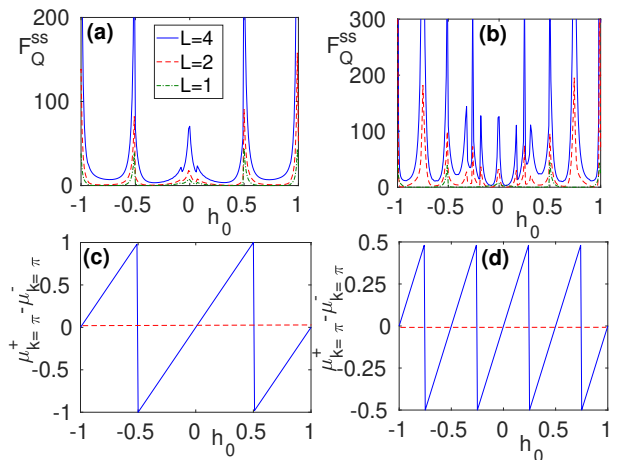


FIG. 3: The QFI in the steady-state with respect to h_0 for different frequency: (a) $\omega=1$; and (b) $\omega=0.5$. The difference of Floquet quasienergies $\mu_{k=\pi}^\pm$ for frequencies: (c) $\omega=1$, and (d) $\omega=0.5$. In all panels, $N=6000$, $h_1=1.5$ and $\gamma=1$.

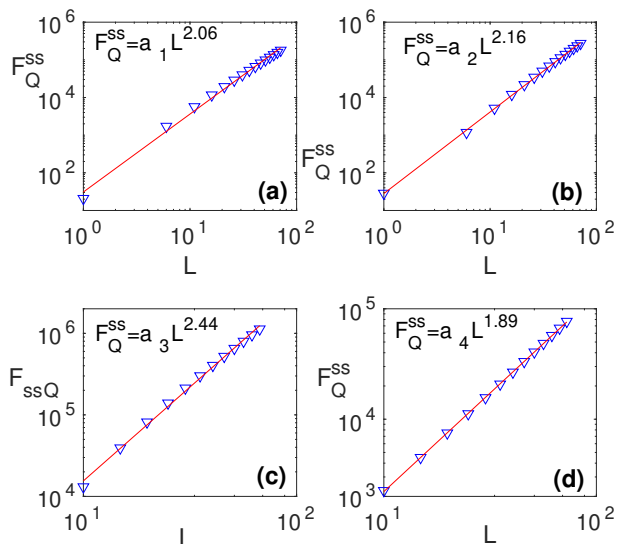


FIG. 4: Scaling of the F_Q^{ss} vs L along the vanishing Floquet quasienergy gap line for: (a) $(\omega, h_0)=(2, 1)$; (b) $(\omega, h_0)=(1, 1)$; (c) $(\omega, h_0)=(0.5, 1)$; and (d) $(\omega, h_0)=(1, 0.5)$. The coefficients are: $a_1=3.43$, $a_2=3.33$, $a_3=3.78$, and $a_4=3.15$. In all panels, $\gamma=1$, $h_1=1.5$.

behavior as F_Q^{gs} in Figs. 1(a)-(b), except around $\gamma=0$ (the behavior of F_Q^{ss} as a function of γ is discussed in the SM). In Fig. 2(d), we plot the F_Q^{ss} for a lower frequency ($\omega=2$). Interestingly the F_Q^{ss} becomes non-zero along the line $h_0=0$, whereas it is zero for $\omega=4$. Thus, by properly driving the system, extra peaks appear in the QFI even away from the ground state criticality and thus achieve quantum-enhanced sensing over a wider range.

Floquet resonance.— To investigate the emergence of extra peaks, we fix the parameters $\gamma=1$, $h_1=1$, and plot the F_Q^{ss} as a function of h_0 in Figs. 3(a)-(b) for frequencies $\omega=1$ and $\omega=0.5$, respectively. In each panel, the different curves are for different block size L . It

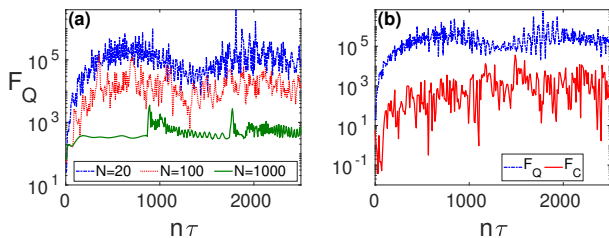


FIG. 5: (a) Dynamics of QFI for different system size N and fixed block-size $L=4$. (b) Dynamics of both quantum and classical Fisher information of a block of $L=4$ for a system of size $N=14$. In all panels, $h_0=1, \gamma=1, h_1=1.5$ and $\omega=1$.

can be seen clearly from the plots that the number of peaks increases as the frequency gets smaller. The peaks are related to the eigenvalues of the one-period Floquet operator $U_k(\tau)$, where $U_k(\tau)$ is the Floquet operator for each quasimomentum mode $k \in [0, \pi]$, as discussed in the SM. The eigenvalues of $U_k(\tau)$ can be written as $e^{i\tau\mu_k^\pm}$ where $\mu_k^\pm = \pm \frac{\omega}{\pi} \tan^{-1} \sqrt{\frac{1-\Re(u_k(\tau))}{1+\Re(u_k(\tau))}}$, are the Floquet quasienergies [34]. Interestingly, the peaks occur at the position of Floquet resonances, i.e., when $\mu_k^+ = \mu_k^-$. For $h_1 \neq 0$, the quasienergy spectrum shows avoided crossing except at $k=0$ and $k=\pi$. Thus, the Floquet resonance condition will only be satisfied by modes at $k=0$ and $k=\pi$. Therefore, the Floquet resonance condition for the energy eigenvalues becomes $2E_{k=0,\pi}(t=0) = q\omega$ for some integer q , where $E_k(t=0) = \pm \sqrt{(h_0 - J \cos(k))^2 + J^2 \gamma^2 \sin^2(k)}$ (see the SM for definition of E_k). We depict the behavior of Floquet quasienergy gap, i.e., $\mu_{k=\pi}^+ - \mu_{k=\pi}^-$ as a function of h_0 for $\omega=1$ and $\omega=0.5$ in Figs. 3(c)-(d), respectively. It can be seen that for each peak in Figs. 3(a)-(b), the quasienergy gap vanishes at those h_0 . Thus, the vanishing of the quasienergy gap is responsible for the peaks in the F_Q^{ss} observed in Figs. 3(a)-(b). The detailed calculation of Floquet formalism and quasienergy gap is provided in the SM.

Driving enhanced sensing.— As seen above, driving the system can enhance the steady-state QFI. It is of utmost interest to see whether this can improve the scaling of the QFI as a function of L . We first focus on the critical point, i.e. $h_0/J=1$, and without loss of generality fix the parameters $\gamma=1$ and $h_1=1.5$. In Figs. 4(a)-(c) we plot F_Q^{ss} versus L together with a power-law fitting function $\tilde{F}_Q^{ss} \sim aL^\eta$ at $h_0/J=1$ for different frequencies such that $F_Q^{ss} \approx \tilde{F}_Q^{ss}$. The coefficient η shows that in the range $\omega \leq 2$ the scaling of the steady-state surpasses the scaling of the ground state. Remarkably, by tuning the driving frequency to $\omega=2$, see Fig. 4(a), one can indeed retrieve the Heisenberg scaling. Further decreasing the frequency can lead to the remarkable super-Heisenberg scaling of $\eta > 2$, showing in Figs. 4(b) and (c). This driving enhanced sensitivity is not limited to the critical point. In Fig. 4(d) we depict the scaling of the QFI versus the

block size L for $\omega=1$ at $h_0/J=0.5$, where the F_Q^{ss} peaks due to Floquet resonance, see Fig. 3(a). Interestingly, the scaling ($\eta=1.8$) exceeds the standard quantum limit showing that quantum-enhanced sensing can be achieved at all Floquet resonances.

Role of the frequency.— As discussed earlier, the enhanced precision is directly related to the vanishing quasienergy gap, which is a function of the frequency of the driving field. In fact, the frequency ω has two roles. First, for $\omega < 2$, the QFI shows extra peaks which are absent in the phase diagram of the ground state, e.g. see Fig. 2(d). Second, at the vanishing Floquet quasienergy gap points, lowering the ω results in better scaling. For instance, as shown in Figs. 4(a)-(c), for the critical field $h_0=1$ one can achieve super-Heisenberg scaling once $\omega < 1$.

Realization in near-term quantum simulators.— Among the emerging quantum simulators ion-traps [71–73] and superconducting devices [74–76] are the best candidates for the realization of our protocol as their interaction can be described by the Hamiltonian in Eq. (1). Near-term quantum devices and simulators are limited in size [77]. To investigate the performance of our protocol on small systems, in Fig. 5(a) we plot F_Q for a block of size $L=4$ as a function of time for various total system sizes. Interestingly, small systems provide high quantum Fisher information indicating more potential for sensing. It is because the larger the system, the more degrees of freedom for the dispersion of information.

It is worth emphasizing that F_Q provides an ultimate bound for sensing precision attained only if the measurement basis is optimal. However, the optimal measurement basis might be complicated and depends on the unknown parameter that makes the saturation of the Cramér-Rao bound very challenging. Here, we consider a simple (but non-optimal) block magnetization measurement along the x direction and compute its corresponding classical Fisher information F_C (the definition of F_C is in the SM). In Fig. 5(b), we plot both F_C and F_Q for a block of size $L=4$ as a function of time in a system of length $N=14$. Interestingly, the F_C not only follows the behavior of F_Q but also takes high values. It shows that a simple non-optimal measurement can serve for sensing.

Conclusion.— In this letter, we have shown that in the absence of global accessibility of the whole state, the Heisenberg scaling of the QFI for the critical many-body ground states of integrable systems reduces to sub-Heisenberg. To retrieve the Heisenberg scaling, we proposed to drive the system using a periodic field and use the steady-state of a block for sensing. Our results show that by tuning the frequency of the periodic field, one can generate multiple peaks across the phase diagram, improves the sensing over a larger interval. The scaling at all these peaks exceeds the standard limit precision and shows significant enhancement compared to the ground state. Remarkably, at lower frequencies, one can even achieve super-Heisenberg scaling for the QFI.

This steady-state quantum-enhanced sensitivity can be explained by the closing of the Floquet quasienergy gap. The protocol is general to all integrable models and best suited for ion traps and superconducting devices in which even a simple non-optimal measurement, such as block magnetization, can be used for achieving high precision.

Acknowledgment.— AB thanks the National Key R&D Program of China (Grant No.2018YFA0306703) and National Science Foundation of China (Grants No.12050410253 and No.92065115) for their support. UM acknowledges funding from the Chinese Postdoctoral Science Fund 2018M643437.

* Electronic address: abolfazl.bayat@uestc.edu.cn

- [1] M. Oszmaniec, R. Augusiak, C. Gogolin, J. Kołodyński, A. Acín, and M. Lewenstein, Random bosonic states for robust quantum metrology. *Phys. Rev. X* **6**, 041044 (2016).
- [2] C. Degen, F. Reinhard, and P. Cappellaro, Quantum sensing. *Rev. Mod. Phys.* **89**, 035002 (2017).
- [3] D. Braun, G. Adesso, F. Benatti, R. Floreanini, U. Marzolino, M. W. Mitchell, and S. Pirandola, Quantum enhanced measurements without entanglement. *Rev. Mod. Phys.* **90**, 35006 (2018).
- [4] L. Pezzé, A. Smerzi, M. K. Oberthaler, R. Schmied, and P. Treutlein, Quantum metrology with nonclassical states of atomic ensembles. *Rev. Mod. Phys.* **90**, 035005 (2018).
- [5] K. Y. Yip, K. On Ho, K. Y. Yu, Y. Chen, W. Zhang, S. Kasahara, Y. Mizukami, T. Shibauchi, Y. Matsuda, S. K. Goh, and S. Yang, Quantum sensing of local magnetic field texture in strongly correlated electron systems under extreme conditions. *Science* **366**, 1355 (2019).
- [6] A. Kuwahata, T. Kitaizumi, K. Saichi, T. Sato, R. Igarashi, T. Ohshima, Y. Masuyama, T. Iwasaki, M. Hatano, F. Jelezko, M. Kusakabe, T. Yatsui, and M. Sekino, Magnetometer with nitrogen-vacancy center in a bulk diamond for detecting magnetic nanoparticles in biomedical applications. *Sci. Rep.* **10**, 2483 (2020).
- [7] J. Smits, J. T. Damron, P. Kehayias, A. F. McDowell, N. Mosavian, I. Fescenko, N. Ristoff, A. Laraoui, A. Jarmola, and V. M. Acosta, Two-dimensional nuclear magnetic resonance spectroscopy with a microfluidic diamond quantum sensor. *Science Advances* **5** eaaw7895 (2019).
- [8] J. Casanova, E. Torrontegui, M. B. Plenio, J. J. García-Ripoll, and E. Solano, Modulated continuous wave control for energy-efficient electron-nuclear spin coupling. *Phys. Rev. Lett.* **122**, 010407 (2019).
- [9] S. L. Braunstein and C. M. Caves, Statistical distance and the geometry of quantum states. *Phys. Rev. Lett.* **72**, 3439 (1994).
- [10] M. G. A. Paris Quantum estimation for quantum technology. *Int. J. Quant. Inf.* **7**, 125 (2009).
- [11] V. Giovannetti, S. Lloyd, and L. Maccone, Quantum-enhanced measurements: beating the standard quantum limit. *Science* **306**, 1330 (2004).
- [12] V. Giovannetti, S. Lloyd, and L. Maccone, Quantum metrology. *Phys. Rev. Lett.* **96**, 010401 (2006).
- [13] F. Fröwis and W. Dür, Stable macroscopic quantum superpositions. *Phys. Rev. Lett.* **106**, 110402 (2011).
- [14] D. Dobrzanski, J. Kołodyński, and M. Guta, The elusive Heisenberg limit in quantum enhanced metrology. *Nat. Commun.* **3**, 1063 (2012).
- [15] H. Kwon, K. C. Tan, T. Volkoff, and H. Jeong, Nonclassicality as a quantifiable resource for quantum metrology. *Phys. Rev. Lett.* **122**, 040503 (2019).
- [16] J. P. Dowling, Quantum optical metrology - the lowdown on high-N00N states. *Contemp. Phys.* **49**, 125 (2008).
- [17] J. Joo, W. J. Munro, and T. P. Spiller, Quantum metrology with entangled coherent states. *Phys. Rev. Lett.* **107**, 083601 (2011).
- [18] S. Slussarenko, M. M. Weston, H. M. Chrzanowski, L. K. Shalm, V. B. Verma, S. W. Nam, and G. J. Pryde, Unconditional violation of the shot-noise limit in photonic quantum metrology. *Nature Photonics* **11**, 700 (2017).
- [19] C. Bonato, M. S. Blok, H. T. Dinani, D. W. Berry, M. L. Markham, D. J. Twitchen, and R. Hanson, Optimized quantum sensing with a single electron spin using real-time adaptive measurements. *Nat. Nanotechnol.* **11**, 247 (2016).
- [20] R. S. Said, D. W. Berry, and J. Twamley Nanoscale magnetometry using a single-spin system in diamond. *Phys. Rev. B* **83**, 125410 (2011).
- [21] B. L. Higgins, D. W. Berry, S. D. Bartlett, H. M. Wiseman, and G. J. Pryde, Entanglement-free Heisenberg-limited phase estimation. *Nature* **450**, 396 (2007).
- [22] D. W. Berry, B. L. Higgins, S. D. Bartlett, M. W. Mitchell, G. J. Pryde, and H. M. Wiseman, How to perform the most accurate possible phase measurements. *Phys. Rev. A* **80**, 052114 (2009).
- [23] B. L. Higgins, D. W. Berry, S. D. Bartlett, M. W. Mitchell, H. M. Wiseman, and G. J. Pryde, Demonstrating Heisenberg-limited unambiguous phase estimation without adaptive measurements. *New J. Phys.* **11**, 073023 (2009).
- [24] S. Gammelmark and K. Mølmer, Remote quantum sensing with Heisenberg limited sensitivity in many body systems. *Phys. Rev. Lett.* **112**, 170401 (2014).
- [25] G. S. Jones, S. Bose, and A. Bayat, Remote quantum sensing with Heisenberg limited sensitivity in many body systems. *arXiv:2003.02308*.
- [26] P. Zanardi and N. Paunković, Ground state overlap and quantum phase transitions. *Phys. Rev. E* **74**, 031123 (2006).
- [27] P. Zanardi, H. T. Quan, X. Wang, and C. P. Sun, Mixed-state fidelity and quantum criticality at finite temperature. *Phys. Rev. A* **75**, 032109 (2007).
- [28] P. Zanardi, M. G. A. Paris, and L. Campos Venuti, Quantum criticality as a resource for quantum estimation. *Phys. Rev. A* **78**, 042105 (2008).
- [29] C. Invernizzi, M. Korbman, L. C. Venuti, and M. G. A. Paris, Optimal quantum estimation in spin systems at criticality. *Phys. Rev. A* **78**, 042106 (2008).
- [30] M. Skotiniotis, P. Sekatski, and W. Dür, Quantum metrology for the Ising Hamiltonian with transverse magnetic field. *New J. Phys.* **17**, 073032 (2015).
- [31] S.-J. Gu, Fidelity approach to quantum phase transitions. *Int. J. Mod. Phys. B* **24**, 4371 (2010).
- [32] S. Gammelmark and K. Mølmer Phase transitions and Heisenberg limited metrology in an Ising chain interacting with a single-mode cavity field *New J. Phys* **13**, 053035 (2011).
- [33] M. M. Rams, P. Sierant, O. Dutta, P. Horodecki, and J. Zakrzewski, At the limits of criticality-based quantum

- metrology: apparent super-Heisenberg scaling revisited. *Phys. Rev. X* **8**, 021022 (2018).
- [34] A. Russomanno, A. Silva, and G. E. Santoro, Periodic steady regime and interference in a periodically driven quantum system. *Phys. Rev. Lett.* **109**, 257201 (2012).
- [35] D. V. Else, B. Bauer, and C. Nayak, Floquet time crystals. *Phys. Rev. Lett.* **117**, 090402 (2016).
- [36] M. S. Rudner, N. H. Lindner, E. Berg, and M. Levin, Anomalous edge states and the bulk-edge correspondence for periodically driven two-dimensional systems. *Phys. Rev. X* **3**, 031005 (2020).
- [37] M. Thakurathi, A. A. Patel, D. Sen, and A. Dutta Floquet generation of Majorana end modes and topological invariants. *Phys. Rev. B* **88**, 155133 (2013).
- [38] T. J. G. Apollaro, G. M. Palma, and J. Marino, Entanglement entropy in a periodically driven quantum Ising chain. *Phys. Rev. B* **94**, 134304 (2016).
- [39] A. Russomanno, G. E. Santoro, and R. Fazio, Entanglement entropy in a periodically driven Ising chain. *J. Stat. Mech.* **7**, 073101 (2016).
- [40] A. Sen, S. Nandy, and K. Sengupta, Entanglement generation in periodically driven integrable systems: dynamical phase transitions and steady state. *Phys. Rev. B* **94**, 214301 (2016).
- [41] S. Lorenzo, J. Marino, F. Plastina, G. M. Palma, and T. J. G. Apollaro, Quantum critical scaling under periodic driving. *Sci. Rep.* **7**, 5672 (2017).
- [42] U. Mishra, R. Prabhu, and D. Rakshit, Quantum correlations in periodically driven spin chains: Revivals and steady-state properties. *J. Magn. Magn. Mater.* **491**, 165546 (2019).
- [43] J. E. Lang, R. B. Liu, and T. S. Monteiro, Dynamical-Decoupling-Based Quantum Sensing: Floquet Spectroscopy. *Phys. Rev. X* **5**, 041016 (2015).
- [44] J. V. Koski, A. J. Landig, A. Pályi, P. Scarlino, C. Reichl, W. Wegscheider, G. Burkard, A. Wallraff, K. Ensslin, and T. Ihn, Floquet spectroscopy of a strongly driven quantum dot charge qubit with a microwave resonator. *Phys. Rev. Lett.* **121**, 043603 (2018).
- [45] V. Mukherjee, A. Zwick, A. Ghosh, Xi Chen, and G. Kurizki, Enhanced precision bound of low-temperature quantum thermometry via dynamical control. *Commun. Phys.* **2**, 162 (2019).
- [46] K. Yang, L. Zhou, W. Ma, Xi Kong, P. Wang, Xi Qin, X. Rong, Ya Wang, F. Shi, J. Gong, and J. Du, Floquet dynamical quantum phase transitions. *Phys. Rev. B* **100**, 085308 (2019).
- [47] R. Jafari and A. Akbari, Floquet dynamical phase transition and entanglement spectrum. *Phys. Rev. A* **103**, 012204 (2021).
- [48] S. Zamani, R. Jafari, and A. Langari, Floquet dynamical quantum phase transition in the extended XY model: nonadiabatic to adiabatic topological transition. *To appear in Phys. Rev. B*.
- [49] K. Mallayya and M. Rigol, Heating rates in periodically driven strongly interacting quantum many-body systems. *Phys. Rev. Lett.* **123**, 240603 (2019).
- [50] T. Ishii, T. Kuwahara, T. Mori, and N. Hatano, Heating in integrable time-periodic systems. *Phys. Rev. Lett.* **120**, 220602 (2018).
- [51] T. Brydges, A. Elben, P. Jurcevic, B. Vermersch, C. Maier, B. P. Lanyon, P. Zoller, R. Blatt, and C. F. Roos, Probing entanglement entropy via randomized measurements. *Science* **364**, 260 (2019).
- [52] U. Mishra and A. Bayat, Integrable quantum many-body sensors for AC field sensing. *arXiv:2105.13507*.
- [53] S. Sachdev, *Quantum Phase Transitions* (Cambridge University Press, 2017).
- [54] The Supplementary material, which contains Refs. [55–58], is available at [url]. Its contents include: (i) the analytical treatment of the time-dependent Hamiltonian; (ii) computing the quantum Fisher information; and (iii) investigating the role of the initial state.
- [55] E. Lieb, T. Schultz, and D. Mattis, Two soluble models of an antiferromagnetic chain. *Annals of Physics* **16**, 407 (1961).
- [56] P. Pfeuty, The one-dimensional Ising model with a transverse field. *Annals of Physics* **57**, 79 (1970).
- [57] A. Carollo, B. Spagnolo, and D. Valenti, Symmetric logarithmic derivative of fermionic gaussian states *Entropy* **12**, 34 (2019).
- [58] D. Šafránek, Discontinuities of the quantum Fisher information and the Bures metric. *Phys. Rev. A* **95**, 05232 (2017).
- [59] L. Gong and P. Tong, Fidelity susceptibility, and von Neumann entropy to characterize the phase diagram of an extended Harper model, *Phys. Rev. B* **78**, 115114 (2008).
- [60] D. Schwandt, F. Alet, and S. Capponi, Quantum monte carlo simulations of fidelity at magnetic quantum phase transitions. *Phys. Rev. Lett.* **103**, 170501 (2009).
- [61] A. F. Albuquerque, F. Alet, C. Sire, and S. Capponi, Quantum critical scaling of fidelity susceptibility. *Phys. Rev. B* **81**, 064418 (2010).
- [62] A. Polkovnikov and V. Gritsev, Universal dynamics near quantum critical points, understanding quantum phase transitions a book chapter in "Understanding Quantum Phase Transitions," edited by Lincoln D. Carr (Taylor & Francis, Boca Raton, 2010).
- [63] B. Damski, Fidelity susceptibility of the quantum Ising model in a transverse field: the exact solution. *Phys. Rev. E* **87**, 052131 (2013).
- [64] B. Damski and M. M. Rams, Exact results for fidelity susceptibility of the quantum Ising model: the interplay between parity, system size, and magnetic field. *J. Phys. A* **47**, 025303 (2014).
- [65] A. Langari and A. T. Rezakhan, Quantum renormalization group for ground-state fidelity. *New J. Phys.* **14**, 053014 (2012).
- [66] P. D. Sacramento, N. Paunković, and V. R. Vieira, Fidelity spectrum and phase transitions of quantum systems. *Phys. Rev. A* **84**, 062318 (2011).
- [67] C.-Y. Park, M. Kang, C.-W. Lee, J. Bang, S.-W. Lee, and H. Jeong, Quantum macroscopicity measure for arbitrary spin systems and its application to quantum phase transitions. *Phys. Rev. A* **94**, 052105 (2016).
- [68] W. C. Yu, Y. C. Li, P. D. Sacramento, and H.-Q. Lin, Reduced density matrix and order parameters of a topological insulator. *Phys. Rev. B* **94**, 245123 (2016).
- [69] L. J. Fiderer and D. Braun, Quantum metrology with quantum-chaotic sensors, *Nat. Comm.* **9**, 1351 (2018).
- [70] W. Liu, M. Zhuang, Bo Zhu, J. Huang, and C. Lee, Quantum metrology via chaos in a driven Bose-Josephson system, *Phys. Rev. A* **103**, 023309 (2021).
- [71] C. Monroe, W. C. Campbell, E. E. Edwards, R. Islam, D. Kafri, S. Korenblit, A. Lee, P. Richerme, C. Senko, and J. Smith, Quantum Simulation of Spin Models with

- Trapped Ions, *Proceedings of the International School of Physics 'Enrico Fermi,' Course 189*, edited by M. Knoop, I. Marzoli, and G. Morigi, 169-187 (2015).
- [72] J. I. Cirac and P. Zoller, Goals and opportunities in quantum simulation, *Nat. Phys.* **8**, 264 (2012).
- [73] R. Blatt and C. F. Roos, Quantum simulations with trapped ions, *Nat. Phys.* **8**, 277 (2012).
- [74] Q. Guo, C. Cheng, Z.-H. Sun, Z. Song, H. Li, Z. Wang, W. Ren, H. Dong, D. Zheng, Y. Zhang, R. Mondaini, H. Fan & H. Wang, Observation of energy-resolved many-body localization, *Nat. Phys.* **17**, 234 (2021).
- [75] M. Gong, G. D. Neto, C. Zha, Y. Wu, H. Rong, Y. Ye, S. Li, Q. Zhu, S. Wang, Y. Zhao, F. Liang, J. Lin, Y. Xu, C.-Z. Peng, H. Deng, A. Bayat, X. Zhu, J.-W. Pan, Experimental characterization of quantum many-body localization transition, arXiv:2012.11521.
- [76] P. Roushan, *et. al.*, Spectroscopic signatures of localization with interacting photons in superconducting qubits, *Science* 358, 1175 (2017).
- [77] J. Preskill Quantum Computing in the NISQ era and beyond, *Quantum* **2**, 79 (2018).

Supplementary Material for “Driving enhanced quantum sensing in partially accessible many-body systems”

Utkarsh Mishra¹ and Abolfazl Bayat¹

¹*Institute of Fundamental and Frontier Sciences, University of Electronic Science and Technology of China, Chengdu 610051, China*

A. DIAGONALIZATION OF THE HAMILTONIAN

The Hamiltonian in Eq. (1) of the main text can be diagonalized even in the presence of time-varying field. We first decompose Pauli spin operators in terms of raising and lowering operators σ^\pm as $\sigma^x = \sigma^+ + \sigma^-$ and $\sigma^y = -i(\sigma^+ - \sigma^-)$. We also obtain a transformation for σ^z as $\sigma^z = 2\sigma^+\sigma^- - \mathbb{I}$. In terms of these operators, the Hamiltonian in Eq. (1) can be written as

$$H(t) = -\frac{J}{2} \sum_{i=1}^N \left(\gamma(\sigma_i^+ \sigma_{i+1}^+ + \sigma_{i+1}^- \sigma_i^-) + (\sigma_i^+ \sigma_{i+1}^- + \sigma_{i+1}^- \sigma_i^+) \right) - \sum_i \frac{(h_0 + h(t))}{2} (2\sigma^+ \sigma^- - \mathbb{I}). \quad (\text{S1})$$

The raising and lowering operators satisfy the anti-commutation relation, $\{\sigma_i^-, \sigma_j^+\} = \delta_{i,j}$, with $(\sigma_i^+)^2 = 0 = (\sigma_i^-)^2$. Thus, the operator σ^\pm partly resemble the Fermi operators. Moreover, they also satisfy $[\sigma_i^+, \sigma_j^-] = [\sigma_i^-, \sigma_j^+] = [\sigma_i^-, \sigma_j^-] = 0$ for $i \neq j$. It can be noticed that the problem of diagonalizing H remains intact as principle axis transformation of σ^\pm does not lead to a proper set of operators which satisfy both commutation and anti-commutation relation. It is discovered [S1, S2] that a new set of Fermi operators can be defined in terms of which the Hamiltonian transforms into a simple form. This transformation, known as the Jordan-Wigner transformation, is defined as $\sigma_i^- = \exp[-i \sum_{\ell=1}^{i-1} \sigma_\ell^+ \sigma_\ell^-] c_i$ and $\sigma_i^+ = c_i^\dagger \exp[-i \sum_{\ell=1}^{i-1} \sigma_\ell^+ \sigma_\ell^-]$. The $c_i^\dagger(c_i)$ operators are Fermi operators $\{c_i, c_j^\dagger\} = \delta_{ij}$, $\{c_i^\dagger, c_j^\dagger\} = 0 = \{c_i, c_j\}$. In terms of the new variables $c_i^\dagger(c_i)$, the Hamiltonian becomes

$$H(t) = -\frac{J}{2} \sum_{i=1}^N \left(\gamma(c_i^\dagger c_{i+1}^\dagger + c_{i+1} c_i) + (c_i^\dagger c_{i+1} + c_{i+1}^\dagger c_i) \right) - \sum_i \frac{(h_0 + h(t))}{2} (2c_i^\dagger c_i - \mathbb{I}). \quad (\text{S2})$$

For the above Hamiltonian, one can define a parity operator $\mathcal{P} = \sum_i c_i^\dagger c_i$. The Hamiltonian commutes with \mathcal{P} i.e., $[\mathcal{P}, H] = 0$. Thus, the Hamiltonian can be divided into any one of the parity sectors. We consider even system size and the positive parity sector. Now, it is customary to define Fourier transformation of the operators $c_i^\dagger(c_i)$ as $c_\ell = \frac{1}{N} \sum_k e^{-ik\ell} d_k$ and similarly for c_ℓ^\dagger , where $k = \frac{\pi}{N}, \frac{3\pi}{N}, \dots, \frac{(N-1)\pi}{N}$. The new Hamiltonian can be written as

$$H(t) = -\frac{J}{2} \sum_{k>0} \left(2\gamma \sin(k) (d_k^\dagger d_{-k}^\dagger + d_{-k} d_k) + 2 \cos(k) (d_k^\dagger d_k + d_{-k}^\dagger d_{-k}) \right) - \sum_k \frac{(h_0 + h(t))}{2} (2d_k^\dagger d_k - \mathbb{I}). \quad (\text{S3})$$

By combining the terms and dropping the constant part from the Hamiltonian, we have

$$H(t) = -J \sum_{k>0} \gamma \sin(k) (d_k^\dagger d_{-k}^\dagger + d_{-k} d_k) - \sum_{k>0} \left(h_0 + h(t) - J \cos(k) \right) (d_k^\dagger d_k + d_{-k}^\dagger d_{-k}). \quad (\text{S4})$$

Thus, the full Hamiltonian is expressed as sum of Hamiltonian $H_k(t)$ for each mode. By rotating d_k and d_k^\dagger as $d_k = \cos(\theta_k)B_k - \sin(\theta_k)B_{-k}$ with $\{B_k, B_{k'}^\dagger\} = \delta_{kk'}$, $\{B_k, B_{k'}\} = 0$, the Hamiltonian can be diagonalized at each instant t as

$$H(t) = \sum_k E_k(t)(2B_k^\dagger B_k - \mathbb{I}), \quad (\text{S5})$$

where, $E_k(t) = \pm \sqrt{(h_0 + h(t) - J \cos(k))^2 + J^2 \gamma^2 (\sin(k))^2}$, is the instantaneous energy and $\theta_k = \tan^{-1} \frac{J \gamma \sin(k)}{h_0 + h(t) - J \cos(k)}$. The ground state spectrum is given by $E_k(t=0)$.

We consider that system is initially prepared in the ground state of $H(0)$ which is expressed as [S3]

$$|\Psi_0\rangle = \bigotimes_k \left(v_k(0)|0\rangle + u_k(0)d_k^\dagger d_{-k}^\dagger |0\rangle \right), \quad (\text{S6})$$

where, $u_k(0) = \sin(\theta_k/2)$ and $v_k(0) = \cos(\theta_k/2)$ with $\theta_k = \tan^{-1} \frac{\gamma \sin(k)}{h_0 - \cos(k)}$. Due to the presence of the probe field $h(t)$ the initial state evolves to $|\Psi(t)\rangle = U(t)|\Psi_0\rangle = \bigotimes_k \left(v_k(t)|0\rangle + u_k(t)d_k^\dagger d_{-k}^\dagger |0\rangle \right)$. The propagator $U(t)$ is given by $U(t) = \mathcal{T} e^{-i \int_0^t H(s) ds}$, where \mathcal{T} is the time-ordered product. Since all the H_k 's are commuting, we have $U(t) = \bigotimes_k U_k(t)$, where $U_k(t) = \mathcal{T} e^{-i \int_0^t H_k(s) ds}$. For stroboscopic dynamics, i.e., $t = n\tau$ and $n \in \mathbb{Z}^+$, $|\Psi(t)\rangle$ can be determined from one the time-period propagator $U(\tau)$. The Floquet theorem allows us to write $U_k(n\tau) = \sum_{\alpha=\pm} e^{-i\mu_k^\alpha n\tau} |\mu_k^\alpha\rangle \langle \mu_k^\alpha|$, where $|\mu_k^\alpha\rangle$ are the Floquet modes with μ_k^α being the Floquet quasienergies [S4]. The μ_k^α 's are unique only when $\mu_k^\alpha \in [-\omega/2, \omega/2]$ and repeats such that $\mu_k^{\alpha, \ell} = \mu_k^\alpha + \ell\omega$, $\ell \in \mathbb{Z}$. The above analysis provide us $|\Psi(n\tau)\rangle = \sum_k \sum_{\alpha=\pm} e^{-i\mu_k^\alpha n\tau} |\mu_k^\alpha\rangle \langle \mu_k^\alpha | \Psi_0\rangle$. Since $U_k \in \text{SU}(2)$, it can be written as $U_k(\tau) = \begin{pmatrix} u_k(\tau) & -v_k^*(\tau) \\ v_k(\tau) & u_k(\tau) \end{pmatrix}$.

Therefore, we can have $\mu_k^\pm = \pm \frac{\omega}{\pi} \tan^{-1} \sqrt{\frac{1 - \Re(u_k(\tau))}{1 + \Re(u_k(\tau))}}$, where \Re stands for the real parts.

B. QUANTUM FISHER INFORMATION IN THE GROUND STATE

We analyze the quantum Fisher information, F_Q^{gs} , of the full chain in the ground state of the model. We focus on the critical point h_0 and obtained F_Q^{gs} as a function of the total system size N . Then, we fit the data on the function of the form $\tilde{F}_Q^{gs} = aN^\eta$ such that $\tilde{F}_Q^{gs} \approx F_Q^{gs}$. The numerical method for obtaining the best fitting function used here is the method of least-square. Once, the best fitting function is obtained, we extract the value of η from the fitting function. In Fig. S1, we perform the fitting and obtained the value of η for two different choices of (h_0, γ) . For $(h_0, \gamma) = (1, 0.5)$ and $(h_0, \gamma) = (1, 1)$, we find that $\eta = 2$ as shown in Figs. S1 (a-b). This is the celebrated Heisenberg scaling of the quantum Fisher information at the second order phase transitions [S5]. In Figs. S1(c-d), we perform scaling for the value of h_0 away from the critical point and the same values of γ i.e., $(h_0, \gamma) = (0.5, 0.5)$ and $(h_0, \gamma) = (0.5, 1)$, we obtained $\eta \approx 1$, which known as the standard quantum limit.

C. STEADY STATE CORRELATION FUNCTIONS AND QUANTUM FISHER INFORMATION OF A BLOCK

To evaluate the reduced density matrix one needs to compute the correlations functions, $\mathcal{C}_{i,j}(t) = \langle \Psi(t) | c_i^\dagger c_j | \Psi(t) \rangle$ and $\mathcal{I}_{i,j}(t) = \langle \Psi(t) | c_i^\dagger c_j^\dagger | \Psi(t) \rangle$ between the fermionic operators, $i, j = 1, \dots, L$. The density matrix $\rho_L(t)$ is then characterized by $\Gamma_{ij}(t) = \langle \Psi(t) | a_i a_j | \Psi(t) \rangle$, where $a_{2i-1} = c_i + c_i^\dagger$ and $a_{2i} = -i(c_i - c_i^\dagger)$ are the Majorana operators, such that $\{a_{2i}, a_{2j}\} = \{a_{2i-1}, a_{2j-1}\} = 2\delta_{i,j}$, $\{a_{2i}, a_{2j-1}\} = 0$, and $i, j = 1, \dots, L$. The time-dependent reduced density matrix, $\rho_L(t)$, can be obtained from the correlations \mathcal{C}_{ij} and \mathcal{I}_{ij} defined as

$$\begin{aligned} \mathcal{C}_{i,j}(t) &= \frac{2}{N} \sum_{k>0} \cos(k(i-j)) \langle d_k^\dagger d_k \rangle_t, \\ \mathcal{I}_{i,j}(t) &= \frac{2i}{N} \sum_{k>0} \sin(k(i-j)) \langle d_k^\dagger d_{-k}^\dagger \rangle_t, \end{aligned} \quad (\text{S7})$$

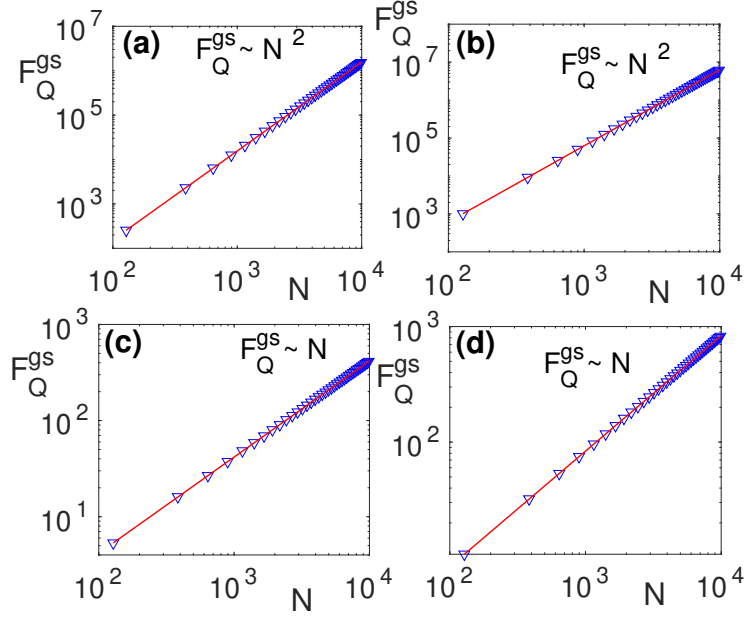


FIG. S1: Scaling of quantum Fisher information, F_Q , as a function of N for (a) $h_0 = 1, \gamma = 0.5$, (b) $h_0 = 1, \gamma = 1$, (c) $h_0 = 0.5, \gamma = 0.5$, and (d) $h_0 = 0.5, \gamma = 1$.

where, $\langle \dots \rangle_t$ is the expectation value taken in the time-evolved state. Now we observed that the evolution operator, $U_k(t)$, can be expressed in terms of its spectral decomposition as

$$U_k(t) = e^{-i\mu_+ t} |\mu_k^+\rangle \langle \mu_k^+| + e^{-i\mu_- t} |\mu_k^-\rangle \langle \mu_k^-|. \quad (\text{S8})$$

With this, we find the $\mathcal{C}_{i,j}(t)$ and $\mathcal{I}_{i,j}(t)$ as

$$\begin{aligned} \mathcal{C}_{i,j}(t) &= \frac{2}{N} \sum_{k>0} \cos(k(i-j)) \langle \psi_k^0 | U_k^\dagger(t) d_k^\dagger d_k U_k(t) | \psi_k^0 \rangle \\ &= \frac{2}{N} \sum_{k>0} \cos(k(i-j)) \left[r_k^+ r_k^{*+} \langle \mu_k^+ | d_k^\dagger d_k | \mu_k^+ \rangle \right. \\ &\quad + r_k^- r_k^{*-} \langle \mu_k^- | d_k^\dagger d_k | \mu_k^- \rangle \\ &\quad + e^{i(\mu_k^+ - \mu_k^-)t} r_k^+ r_k^{*-} \langle \mu_k^+ | d_k^\dagger d_k | \mu_k^- \rangle \\ &\quad \left. + e^{i(\mu_k^- - \mu_k^+)t} r_k^- r_k^{*+} \langle \mu_k^- | d_k^\dagger d_k | \mu_k^+ \rangle \right]. \end{aligned} \quad (\text{S9})$$

$$\begin{aligned} \mathcal{I}_{i,j}(t) &= \frac{2i}{N} \sum_{k>0} \sin(k(i-j)) \langle \psi^0 | U_k^\dagger d_k^\dagger d_{-k}^\dagger U_k | \psi^0 \rangle \\ &= \frac{2i}{N} \sum_{k>0} \sin(k(i-j)) \left[r_k^+ r_k^{*+} \langle \mu_k^+ | d_k^\dagger d_{-k}^\dagger | \mu_k^+ \rangle \right. \\ &\quad + r_k^- r_k^{*-} \langle \mu_k^- | d_k^\dagger d_{-k}^\dagger | \mu_k^- \rangle \\ &\quad + e^{i(\mu_k^+ - \mu_k^-)t} r_k^+ r_k^{*-} \langle \mu_k^+ | d_k^\dagger d_{-k}^\dagger | \mu_k^- \rangle \\ &\quad \left. + e^{i(\mu_k^- - \mu_k^+)t} r_k^- r_k^{*+} \langle \mu_k^- | d_k^\dagger d_{-k}^\dagger | \mu_k^+ \rangle \right]. \end{aligned} \quad (\text{S10})$$

Note that $|\Psi_0(0)\rangle = \otimes_k |\psi_k^0\rangle$ is the initial state and $r_k^\pm = \langle \psi_k^0 | \mu_k^\pm \rangle$, describes the overlap of the initial state with that of the Floquet eigenstates. Taking the limit $t \rightarrow \infty$ and $N \rightarrow \infty$, we obtain the correlation functions in the steady-state

as

$$\begin{aligned} \mathcal{C}_{i,j}^\infty &= \frac{1}{\pi} \int_0^\pi dk \cos(k(i-j)) \left[|r_k^+|^2 \langle \mu_k^+ | d_k^\dagger d_k | \mu_k^+ \rangle \right. \\ &\quad \left. + |r_k^-|^2 \langle \mu_k^- | d_k^\dagger d_k | \mu_k^- \rangle \right], \end{aligned} \quad (\text{S11})$$

$$\begin{aligned} \mathcal{I}_{i,j}^\infty &= \frac{i}{\pi} \int_0^\pi dk \sin(k(i-j)) \left[|r_k^+|^2 \langle \mu_k^+ | d_k^\dagger d_{-k}^\dagger | \mu_k^+ \rangle \right. \\ &\quad \left. + |r_k^-|^2 \langle \mu_k^- | d_k^\dagger d_{-k}^\dagger | \mu_k^- \rangle \right], \end{aligned} \quad (\text{S12})$$

where we replace the summation by integration. The non-zero elements of the Γ matrix, therefore, are given by

$$\begin{aligned} \Gamma_{2i-1,2j-1} &= \delta_{i,j} + 2i\Im(\mathcal{C}_{i,j} + \mathcal{I}_{i,j}) \\ \Gamma_{2i-1,2j} &= i\delta_{i,j} - 2i\Re(\mathcal{C}_{i,j} - \mathcal{I}_{i,j}) \\ \Gamma_{2i,2j-1} &= -i\delta_{i,j} + 2i\Re(\mathcal{C}_{i,j} + \mathcal{I}_{i,j}) \\ \Gamma_{2i,2j} &= \delta_{i,j} + 2i\Im(\mathcal{C}_{i,j} - \mathcal{I}_{i,j}). \end{aligned} \quad (\text{S13})$$

Once we obtain the matrix Γ , we can get the quantum Fisher information F_Q of a block of size L [S6, S7] as

$$F_Q(t) = \sum_{r,s=1}^{2L} \frac{\langle r | \partial_{h_0} \Gamma | s \rangle \langle s | \partial_{h_0} \Gamma | r \rangle}{(1 - \lambda_r \lambda_s)}. \quad (\text{S14})$$

Here, $\Gamma = \sum_{r=1}^{2L} \lambda_r |r\rangle \langle r|$ is the spectral decomposition of Γ and $\partial_{h_0} \Gamma = \frac{\partial \Gamma}{\partial h_0}$. The above formula can show singular behavior at $\gamma_r = \gamma_s = \pm 1$. It is shown that the above singularity can be removable [S8].

D. ROLE OF ANISOTROPY IN THE QFI

In Fig. S2, we plot F_Q^{ss} as a function of anisotropy parameter γ for $h_0/J = 1$ for different frequencies, ω . In Fig. S2(a), the F_Q^{ss} is for $L = 4$ and in Fig. S2(b), it is for $L = 20$. It can be seen that as we increase $|\gamma|$, F_Q^{ss} increases monotonically with γ . The F_Q^{ss} shows a peak at some value of γ which depends on the ω . It then decreases with the $|\gamma|$. The steady-state F_Q^{ss} is greater than the ground state F_Q^{gs} for a range of γ . In fact for certain frequencies and block size L , the $F_Q^{ss} > F_Q$ for all γ .

E. FLOQUET THEORY AND FLOQUET RESONANCES

In this sections, we give analytical arguments for the occurrence of Floquet resonances for all values of h_1 . For a time-periodic many-body Hamiltonian, $H(t+\tau) = H(t)$, with periodicity $\tau = 2\pi/\omega$, the solution of the Schrödinger equation follows from the Floquet theorem. The Floquet theorem gives an ansatz of the form $|\Psi(t)\rangle = \sum_\alpha c^\alpha e^{-i\mu^\alpha t} |\Phi^\alpha(t)\rangle$. Here $c^\alpha \in \mathbb{C}$, μ^α are quasienergies, and $|\Phi^\alpha(t)\rangle$ are Floquet modes. Substituting the ansatz to the Schrödinger equation, $H(t)|\Psi(t)\rangle = -i\hbar \frac{\partial |\Psi(t)\rangle}{\partial t}$, the Floquet modes satisfy

$$\left(H(t) - i \frac{\partial}{\partial t} \right) |\Phi^\alpha(t)\rangle = \mu^\alpha |\Phi^\alpha(t)\rangle. \quad (\text{S15})$$

It can be noted that $|\Phi^\alpha(t+\tau)\rangle$ is also a solution of the above equation with quasienergy μ^α , therefore, we have $|\Phi^\alpha(t+\tau)\rangle = |\Phi^\alpha(t)\rangle$. For the model, we consider propagator $U(t) = \mathcal{T} e^{-i \int_0^t H(s) ds}$ so that $U(t+\tau)|\Psi(t)\rangle = |\Psi(t+\tau)\rangle$. Using the ansatz for $|\Psi(t)\rangle$ in the above equation, we have $U(t+\tau)e^{-i\mu^\alpha t} |\Phi^\alpha(t)\rangle = e^{-i\mu^\alpha(t+\tau)} |\Phi^\alpha(t+\tau)\rangle = e^{-i\mu^\alpha(t+\tau)} |\Phi^\alpha(t)\rangle$. This shows that the Floquet modes are eigenvectors of the one time-period propagator $U(\tau)$ and quasienergies μ^α are

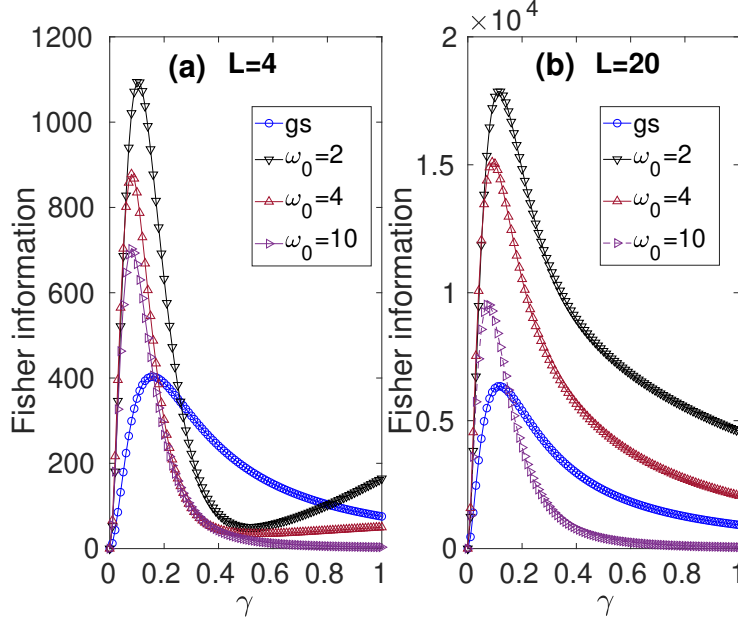


FIG. S2: F_Q^{gs} and F_Q^{ss} as a function of γ for (a) $L = 4$ and (b) $L = 20$. Here $h_0 = 1$, $h_1 = 1.5$, and $N = 6000$.

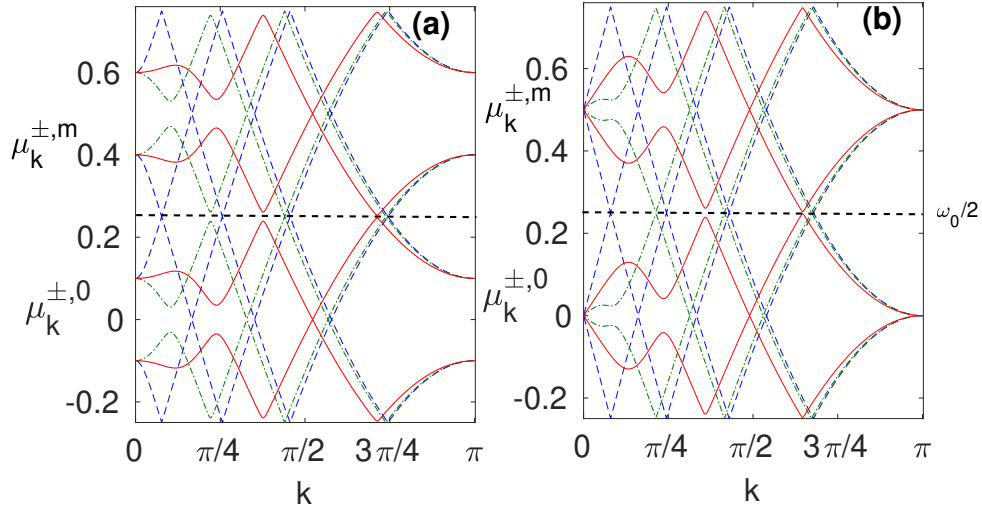


FIG. S3: Quasienergies μ_k^\pm as a function of k for (a) $h_0 = 0.9$ and (b) $h_0 = 1$. The different curves in the panel are for different h_1 : $h_1 = 0.0$ (blue dashed) $h_1 = 0.5$ (green dot dashed), and $h_1 = 1$ (solid red lines). Here $\omega = 0.5$, $h_0 = 1$, $\gamma = 1$, and $m = 1$.

its eigenvalues. We numerically diagonalize the one time-period propagator $U_k(\tau)$ for each 2×2 k -space and obtained the Floquet modes $|\mu_k^\pm\rangle$ and quasienergies μ_k^\pm .

As it has been shown in the main text, Figs. 3(a-b), that there is a peak in F_Q^{ss} for certain h_0 for a fixed ω . In Figs. 3(c-d), we find that the peaks occurs at the point where Floquet gap vanishes. The peaks have also been observed before in the other quantities [S9–S11]. Here, we explain the occurrence of Floquet resonance in the system observed in the QFI following Ref. [S9]. The Floquet modes $|\mu_k^\pm\rangle$ are defined upto a periodic phase, i.e., $|\mu_k^{\pm,\ell}(t)\rangle = e^{i\omega\ell t}|\mu_k^\pm\rangle$, where ℓ is an integer. The new Floquet quasienergies are, therefore, shifted as $\mu_k^{\pm,\ell} = \mu_k^\pm \pm \ell\omega$. Thus, the quasienergies are uniquely defined upto a translation of an integer multiple of ω . It is feasible, therefore, to define the quasienergies within the first Brillouin zone $[-\omega/2, \omega/2]$. In the absence of driving, $h_1 \rightarrow 0$, $U_k(\tau, 0) = e^{-iH_k\tau}$. Thus, for the critical sensing, i.e., for $h_0 = 1$, the Floquet quasienergies are the eigenvalues of the critical H_k . Thus, we have $\mu_k^{\pm,\ell} = \pm 2\gamma \sin(k/2) + \ell\omega$. The degeneracy condition translate into $4\gamma \sin(k/2) = p\omega$, where $p \in \mathbb{N}$. This is known as the n -photon resonance condition. For finite h_1 , and for $h_0 = 0.9$ (different from the value where F_Q^{ss} is peaked), the quasienergies are always gapped for all k , as can be seen from Fig. S3(a). Thus, there will not be any Floquet resonance

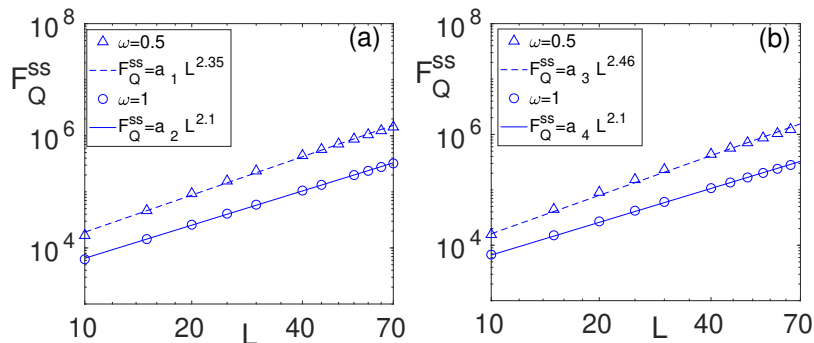


FIG. S4: Fitting of the F_Q^{ss} as a function of L with fitting function $F_Q^{ss} = aL^\eta$ for different initial states: (a) $|\psi_1\rangle = |0 \otimes 0 \otimes \dots \otimes 0\rangle = |0\rangle^{\otimes N}$ and (b) $|\psi_2\rangle = |+\otimes +\otimes \dots \otimes +\rangle = |+\rangle^{\otimes N}$, where $|+\rangle = \frac{1}{\sqrt{2}}(|0\rangle + |1\rangle)$. The fitting coefficients are: $a_1 = 4.208$, $a_2 = 3.74$, $a_3 = 3.76$, and $a_4 = 3.75$. Here $h_0 = 1$, $\gamma = 1$, and $h_1 = 1.5$.

for $h_0 = 0.9$. On the other hand, for $h_1 \neq 0$ and $h_0 = 1$, the quasienergies open a gap at all k except at $k = 0, \pi$, as can be seen from Fig. S3(b). In Fig. S3(b), we plot the quasienergies for various h_1 in the range $[-3\omega/2, \omega/2]$ for $\omega = 0.5$. It can be seen from the plot that by translating $\mu_k^\pm \rightarrow \mu_k^\pm + \omega$, we get the same quasienergies within the range $[-\omega/2, \omega/2]$. Moreover, it can be seen from the plot that as h_1 increases from $h_1 = 0$ to $h_1 = 1$, there is a gap in the quasienergies except at $k = 0, \pi$. To obtain the degeneracy condition for $h_1 \neq 0$, one can first change the system in a rotating frame via a time-dependent transformation $\mathcal{V}(t) = \exp\left(-ih_1 \frac{\cos(\omega t)}{\omega} \sigma^z\right)$. This gives a transformed Hamiltonian $\mathcal{H}_k(t) = \mathcal{V}_k^\dagger(t) H_k(t) \mathcal{V}_k(t) - i\mathcal{V}_k^\dagger(t) \dot{\mathcal{V}}_k(t)$. The new Hamiltonian is $\mathcal{H}_k = (h_0 - J \cos(k))\sigma^z + \gamma\sigma^y \sin(k) \exp\left(2ih_1 \frac{\cos(\omega t)}{\omega}\right)$. Now for the modes for which the amplitude h_1 has small effect on quasienergies can be neglected. Therefore, the second term of \mathcal{H}_k will not contribute in determining the Floquet resonances. The Floquet Hamiltonian (H_k^F), then, can be constructed as

$$e^{-iH_k^F \tau} = \mathcal{T} e^{-i \int_0^\tau H_k(t) dt} \quad (\text{S16})$$

The quasienergies, i.e., the eigenvalues of H_k^F , are given by $\mu_{k=0}^{\pm, \ell} = \pm(h_0 - h_c) + \ell\omega$ and $\mu_{k=\pi}^{\pm, \ell} = \pm(h_0 + h_c) + \ell\omega$ upto the translation of an integer multiple of ω . It can be noted that $\pm(h_0 - h_c) + \ell\omega$ and $\pm(h_0 + h_c) + \ell\omega$ are also the eigenvalues of $\mathcal{H}_{k=0}(t)$ and $\mathcal{H}_{k=\pi}(t)$, respectively. The degeneracy condition of quasienergies gives $2(h_0 \pm h_c) = q\omega$ with $q \in \mathbb{N}$, which is equivalent to $E_{k=0, \pi}(t=0) = q\omega$.

F. CLASSICAL FISHER INFORMATION

The classical Fisher information F_C with respect to the parameter h_0 is defined as

$$F_C = \sum_i \frac{1}{p_i} \left(\frac{\partial p_i}{\partial h_0} \right)^2, \quad (\text{S17})$$

where p_i 's are the probabilities of a positive operator valued measurement (POVM) such that each $p_i > 0$ and $\sum_i p_i = 1$. For the present case, we consider a simple, though sub-optimal, measurement which is independent of h_0 . The measurement is the block magnetization along x -direction for a block of size L . For a block of size L , the global magnetization takes $L+1$ outcomes from $O_1 = +L$ (when all the qubits are $|+\rangle$), $O_2 = L-2$ (when except one qubit the rest are in the state $|+\rangle$) until $O_{L+1} = -L$ (when all the qubits are $|-\rangle$). Here $|\pm\rangle = \frac{1}{\sqrt{2}}(|0\rangle \pm |1\rangle)$. Each of the outcomes O_r has probability p_r of occurrence. Then one can use Eq. (S17) to get the corresponding classical Fisher information F_C .

G. ROLE OF THE INITIAL STATE

In this section, we present results for the scaling of the F_Q^{ss} for the two initial states (i) $|\psi_1\rangle = |0 \otimes 0 \otimes \dots \otimes 0\rangle = |0\rangle^{\otimes N}$ and (ii) $|\psi_2\rangle = |+\otimes +\otimes \dots \otimes +\rangle = |+\rangle^{\otimes N}$, where $|+\rangle = \frac{1}{\sqrt{2}}(|0\rangle + |1\rangle)$ and $\sigma^z|0\rangle = |0\rangle$ and $\sigma^z|1\rangle = -|1\rangle$. In Fig. S4, we show scaling of the F_Q^{ss} with subsystem size L at $h_0 = 1$ for $|\psi_1\rangle$ in Fig. S4 (a) and $|\psi_2\rangle$ in Fig. S4 (b). From the

obtained scaling exponent η using method of least square fitting, we found that the scaling exponent is almost same for all the initial states considered. Thus, we can conclude that the scaling behavior is independent of the initial state and depend on the occurrence of vanishing Floquet gap as discussed in the main text.



* Electronic address: abolfazl.bayat@uestc.edu.cn

- [S1] E. Lieb, T. Schultz, and D. Mattis, Two soluble models of an antiferromagnetic chain. *Annals of Physics* **16**, 407 (1961).
- [S2] P. Pfeuty, The one-dimensional Ising model with a transverse field. *Annals of Physics* **57**, 79 (1970).
- [S3] S. Sachdev, *Quantum Phase Transitions* (Cambridge University Press, 2017).
- [S4] We obtained the quasienergies by diagonalizing $A = -1(\mathbb{I} - U(\tau))(\mathbb{I} + U(\tau))^{-1}$. The quasienergies are given by $\mu_\alpha = (\omega_0/\pi) \tan^{-1}(a_\alpha)$, where $A = \sum_\alpha a_\alpha |a_\alpha\rangle\langle a_\alpha|$.
- [S5] P. Zanardi and N. Paunković, Ground state overlap and quantum phase transitions. *Phys. Rev. E* **74**, 031123 (2006).
- [S6] A. Carollo, B. Spagnolo, and D. Valenti, Symmetric logarithmic derivative of fermionic gaussian states *Entropy* **12**, 34 (2019).
- [S7] Utkarsh Mishra and Abolfazl Bayat, Integrable quantum many-body sensors for AC field sensing, arXiv:2105.13507.
- [S8] D. Šafránek, Discontinuities of the quantum Fisher information and the Bures metric. *Phys. Rev. A* **95**, 05232 (2017).
- [S9] A. Russomanno, A. Silva, and G. E. Santoro, Periodic Steady Regime and Interference in a Periodically Driven Quantum System. *Phys. Rev. Lett.* **109**, 257201 (2012).
- [S10] A. Russomanno, G. E. Santoro, and R. Fazio, Entanglement entropy in a periodically driven Ising chain. *J.Stat.Mech.* **7**, 073101 (2016).
- [S11] A. Sen, S. Nandy, and K. Sengupta, Entanglement generation in periodically driven integrable systems: dynamical phase transitions and steady state. *Phys. Rev. B* **94**, 214301 (2016).